Supporting Information

A series of water-soluble A-π-A′ typological indolium derivatives with two-photon properties for rapidly detecting HSO_3^-/SO_3^{2-} in living cells

Yingzhong Zhu[a], Wei Du[a], Mingzhu Zhang[a], Qiong Zhang[a*], Xiaohe Tian[b*], Hongping Zhou[a], Jieying Wu[a], Yupeng Tian[ac*]

[a] *Department of Chemistry, Key Laboratory of Functional Inorganic Material Chemistry of Anhui Province, Anhui University, Hefei 230039, P. R. China*

[b] *School of life science, Anhui University, Hefei 230039, P. R. China*

[c] *State Key Laboratory of Coordination Chemistry, Nanjing University, 210093 Nanjing, P. R. China*

* Corresponding author. Department of Chemistry, Key Laboratory of Functional Inorganic Material Chemistry of Anhui Province, Anhui University, 230039 Hefei, PR China. E-mail address: zhangqiong.314@163.com; yptian@ahu.edu.cn

Content

Two-photon cross-section

Two-photon absorption cross-sections of the samples were obtained by the two-photon excited fluorescence (2PEF) method with fluorescein as reference. The fluorescein was dissolved in NaOH aqueous solution (pH = 13, Φ = 0.95, δ = 38 GM before 850 nm, and δ = 11 GM after 850 nm) with concentration of 5×10^{-4} mol/L in a 1 cm standard quartz cell. The average power used in 2PEF was 200 mW adjusted by a Glan prism. Thus the cross-sections could be measured using the equation below:

$$\delta = \delta_{ref} \frac{\Phi_{ref}}{\Phi} \frac{C_{ref}}{C} \frac{n_{ref}}{n} \frac{F}{F_{ref}}$$

Here, the subscripts *ref* represented for the reference molecule. δ was the 2P absorption cross-section value, c was the concentration of solution, n was the refractive index of the solution, F was the integrated area of the detected two-photon-induced fluorescence signal, and Φ was the fluorescence quantum yield.

Lippert-Magata equation

The Lippert-Mataga equation is shown as follow:

$$\Delta\nu = \frac{2\Delta f}{4\pi\varepsilon_0 hca^3}(\mu_e - \mu_g)^2 + b$$

$$\Delta f = \frac{\varepsilon - 1}{2\varepsilon + 1} - \frac{n^2 - 1}{2n^2 + 1}$$

in which $\Delta\nu = \nu_{abs} - \nu_{em}$ stands for Stokes shift, ν_{abs} and ν_{em} are absorption and emission frequency (cm^{-1}), $\hbar$ is the Plank's constant, c is the velocity of light in vacuum, a is the Onsager radius and b is a constant. Δf is the orientation polarizability, ε is the refractive index, n is the dielectric constant, μ_e and μ_g are the dipole moments of the emissive and ground states, respectively and ε_0 is the permittivity of the vacuum. $(\mu_e-\mu_g)^2$ is proportional to the slope of the Lippert-Mataga plot. The Onsager radius and the dipole moment (μ_g) were obtained by geometry optimization using b3lyp/6-31g* method.

MTT method

The cytotoxicitie (IC_{50}) of **L3** was determined using a MTT assay, a standard method to detect cell survival fraction, by incubating cancerous cells (HepG2). The cells were cultured in 96-well

glass-bottom plates for 48 h with the initially cell number 5000 per well. Then the cells were incubated with various concentrations of **L3** (5 μmol/L, 10 μmol/L, 15 μmol/L, and 20 μmol/L) for 24 h. After that, the suspension medium was removed and 10 μL (5 mg/mL in PBS solutions) MTT (5-dimethylthiazol-2-yl-2,5-diphenyltetrazolium bromide) was added to each well and performed for 4 h. When the incubation was finished, culture supernatants were aspirated away and purple formazan crystals were dissolved into 150 μL of DMSO for additional incubation of 15 min. The concentration of the reduced MTT in each well was measured at a reference wavelength of 630 nm while using a test wavelength of 570 nm employing a microplate reader (318C, INESA Instrument, China). The cell viability was estimated according to the following equation:

$$\text{Cell viability (\%)} = OD_{treated}/OD_{control} \times 100\%$$

$OD_{treated}$ was obtained in the presence of **L3**, while $OD_{control}$ was got in the absence of **L3**. The experiments were performed in sextuplicate. The value of $p < 0.05$ was considered in significance.

Confocal microscopy imaging and co-localization with liveing cell

HepG2 and Hela cells were chosen to use in confocal microscopy imaging. The cells were plated in 24 well glass-bottom plates (cellvis) and cultured for 48 h. The cells were solely incubated with 1 mL media containing 1×10^{-5} mol/L of **L3** for 30 min (37 ^{o}C, 5% CO_2). The excess **L3** was washed away by PBS for 3 times, after that the confocal microscopy imaging was carried out. For co-localization, the HepG2 cells were incubated with Mitotracker®Red, LysoTracker® Red DND-99 and NucRed™ Live 647 for 10 min before washed way the excess trackers by PBS for 3 times.

Confocal microscopy imaging was acquired with a Carl Zeiss LSM 710 confocal microscopy and 63 × oil-immersion objective lens. The incubated cells were excited at 405 nm for **L3**, 579 nm for Mitotracker®Red, 543 nm for LysoTracker® Red DND-99, and 618 nm for NucRed™ Live 647 with a semiconductor laser, and the emission signals were collected at 450-490 nm and 560-600 nm for **L3**, 600 ± 20 nm for Mitotracker®Red, 590 ± 20 nm for LysoTracker® Red DND-99, and 640 ± 20 for NucRed™ Live 647, respectively. Two-photon confocal microscopy imaging of **L3** was excited at 840 nm, while the emission signals were detected in the region of 610-650 nm. Quantization by line plots was accomplished by using the software Image J.

Table S1. Summary of ratiometric fluorescence probes based on benzindole derivatives for detecting HSO_3^-/SO_3^{2-}

ID	Probe name	Molecular model	2P probe	Detection time	Detection limit (nM)	Other anions response	Bio-imaging
1	BIFS	A-π-A	No	3 min	3.0	non	yes
2	1	D-π-A	No	1 min	97	HS^-	no
3	DB1/DB2	D-π-A	Yes	/	160/570	non	yes
4	1	A-π-A	No	90 s	5.6	HS^-	no
5	Probe 1	D-π-A	No	50 s	27.6	non	no
6	DCI	D-π-A	No	150 s	30000	non	yes
7	1	A-π-A (complex)	No	/	/	HS^-	no
8	CZBI	D-π-A	No	40 s	10.0	non	yes
9	CY-SO_2	D-π-A	No	90 s	2.6	non	yes
10	NBD-Id-S	D-π-A	No	20 s	3.6	non	yes
11	BCS-1	D-π-A	No	/	72	non	yes

1. Zhu L, Xu J, Sun Z, et al. A twisted intramolecular charge transfer probe for rapid and specific detection of trace biological SO_2 derivatives and bio-imaging applications[J]. Chemical Communications, 2015, 51(6): 1154-1156.
2. Sun Y, Fan S, Zhang S, et al. A fluorescent turn-on probe based on benzo[e]indolium for bisulfite through 1,4-addition reaction[J]. Sensors and Actuators B: Chemical, 2014, 193: 173-177.
3. Li D, Shi Y, Tian X, et al. Fluorescent probes with dual-mode for rapid detection of SO_2 derivatives in living cells: Ratiometric and two-photon fluorescent sensors[J]. Sensors and Actuators B: Chemical, 2016, 233: 1-6.
4. Sun Y, Zhao D, Fan S, et al. Ratiometric fluorescent probe for rapid detection of bisulfite through 1, 4-addition reaction in aqueous solution[J]. Journal of agricultural and food chemistry, 2014, 62(15): 3405-3409.
5. Xiang K, Chang S, Feng J, et al. A colorimetric and ratiometric fluorescence probe for rapid detection of SO_2 derivatives bisulfite and sulfite[J]. Dyes and Pigments, 2016, 134: 190-197.
6. Wang G, Chen H, Chen X, et al. A novel carbazole-based mitochondria-targeted ratiometric fluorescent probe for bisulfite in living cells[J]. RSC Advances, 2016, 6(22): 18662-18666.
7. Su X, Hu R, Li X, et al. Hydrophilic Indolium Cycloruthenated Complex System for Visual Detection of Bisulfite with a Large Red Shift in Absorption[J]. Inorganic chemistry, 2015, 55(2): 745-754.
8. Xu J, Pan J, Jiang X, et al. A mitochondria-targeted ratiometric fluorescent probe for rapid, sensitive and specific detection of biological SO_2 derivatives in living cells[J]. Biosensors and Bioelectronics, 2016, 77: 725-732.
9. Li H, Yao Q, Fan J, et al. A fluorescent probe for ratiometric imaging of SO_2 derivatives in mitochondria of living cells[J]. Industrial & Engineering Chemistry Research, 2016, 55(6): 1477-1483.
10. Wang Y, Meng Q, Zhang R, et al. A Ratiometric Fluorescence Probe for Imaging of Sulfur Dioxide Derivatives in Mitochondria of Living Cells[J]. Organic & Biomolecular Chemistry, 2017.
11. Yang J, Li K, Hou J T, et al. Novel Tumor-Specific and Mitochondria-Targeted near-Infrared-Emission Fluorescent Probe for SO_2 Derivatives in Living Cells[J]. ACS Sensors, 2015, 1(2): 166-172.

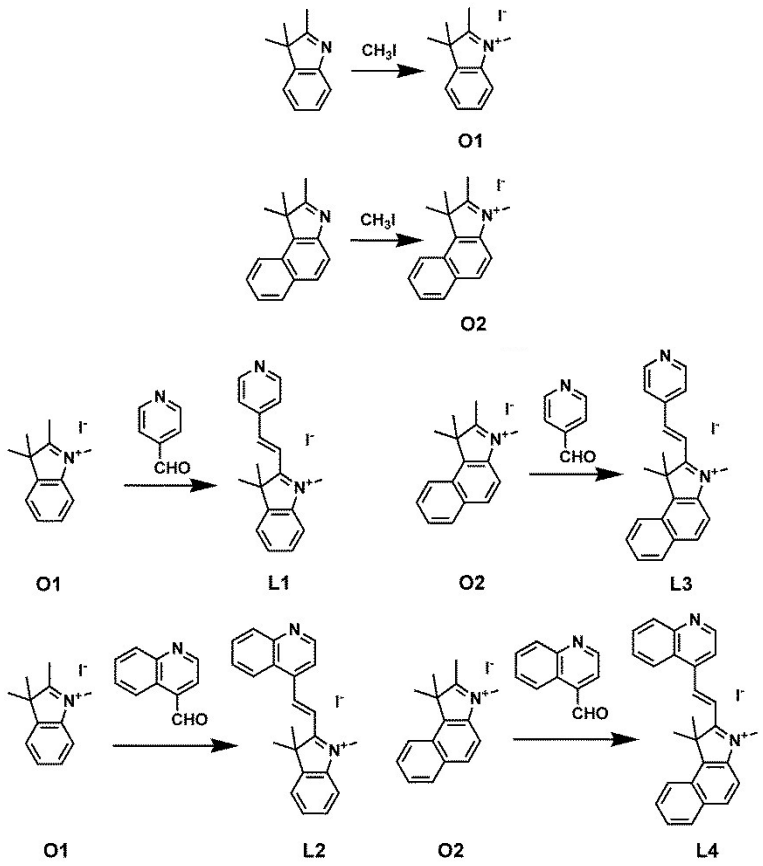

Scheme S1. The synthetic routes for **O1**, **O2**, **L1**, **L2**, **L3**, and **L4**

Table S2. Crystal data collection and structure refinement for **L1**-**L2**

Compounds	**L1**	**L2**
CCDC no.	1523227	1523228
Empirical formula	$C_{18}H_{19}IN_2$	$C_{22}H_{23}I_2N_2O$
Formula weight	390.25	585.22
Temperature	298(2) K	298(2) K
Wavelength	0.71073 Å	0.71069 Å
Space group	$Cmc2_1$	$P2_1/c$
Crystal system	Orthorhombic	Monoclinic
a/Å	7.299(2)	12.632(5)
b/Å	18.472(3)	6.968(5)
c/Å	12.541(2)	24.753(5)
α(°)	/	/

β(°)	90	96.016(5)
γ(°)	/	/
Volume A^3	1690.9(5)	2167(2)
Z	4	4
Dc/Mg m^{-3}	1.533	1.794
μ/mm^{-1}	1.890	2.917
F(000)	776	1132
Final R indices	R1 = 0.0210	R1 = 0.0304
[I > 2σ(I)]	wR2 = 0.0430	wR2 = 0.0870
Goodness-of-fit on F2	1.061	1.047

Table S3. The selected bond length of **L1** and **L2** (Å)

L1		**L2**	
C(5)-C(6)	1.478(6)	C(3)-C(10)	1.462(4)
C(6)-C(7)	1.335(12)	C(10)-C(11)	1.343(5)
C(7)-C(8)	1.437(11)	C(11)-C(12)	1.438(5)
C(8)-N(2)	1.303(5)	C(12)-N(2)	1.325(4)
N(2)-C(11)	1.427(8)	N(2)-C(15)	1.430(5)

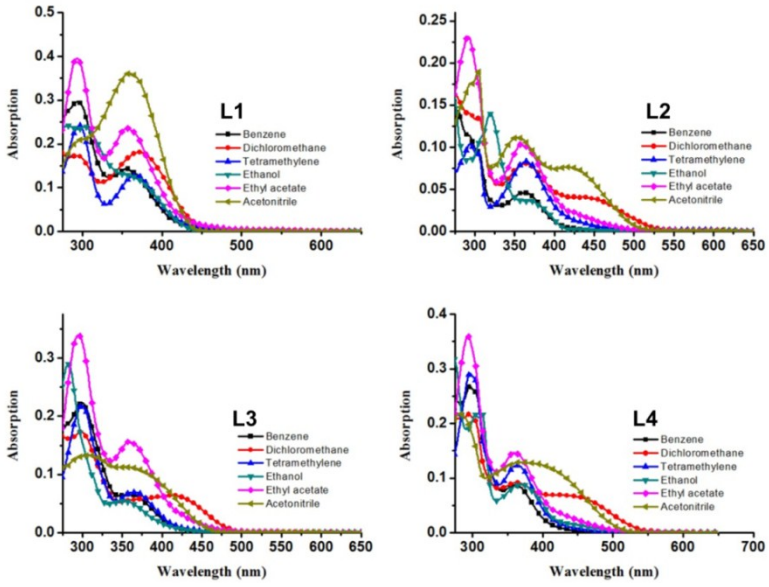

Figure S1. The UV-vis absorption spectra of compounds **L1-L4** in different solvents with concentration 10 μM.

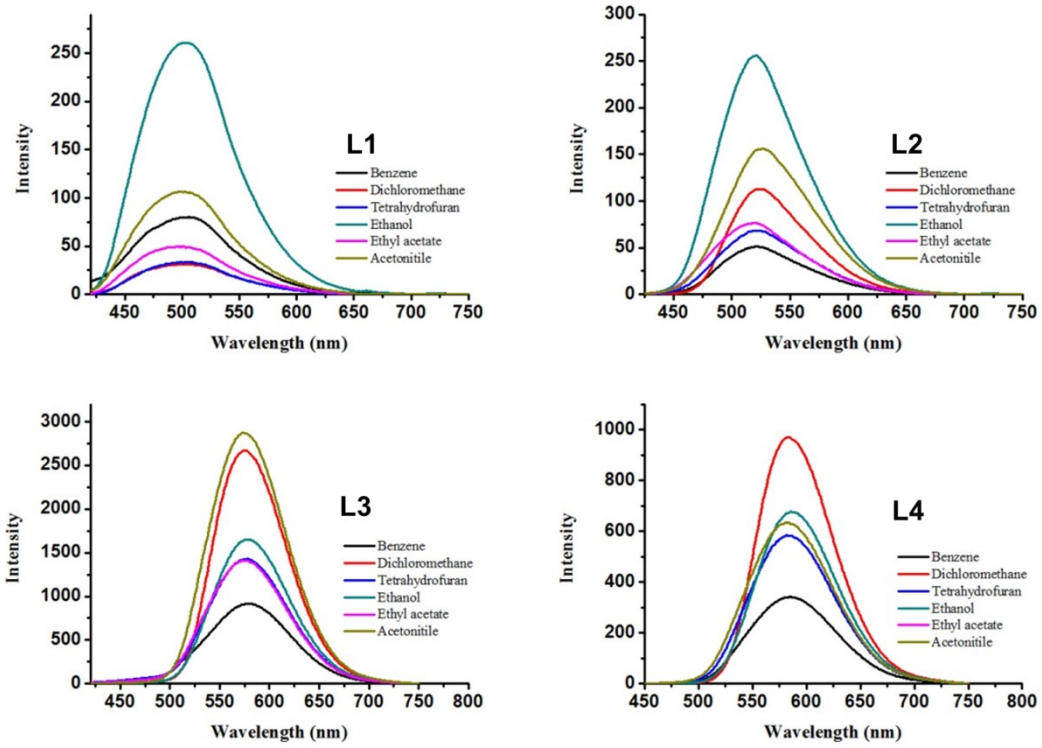

Figure S2. The fluorescence emission spectra of compounds **L1**-**L4** in different solvents with concentration 10 μM.

Table S4. Photophysical data in different solvents

Compounds	Solvents	λ_{max}[a](ε_{max}[b])	λ_{max}[c]	$\Delta\nu$[d]	Φ_f[e] (%)	τ/ns[f]
L1	Benzene	355(1.43)	505	8364	< 1.0	< 0.10
	Dichloromethane	371(1.80)	499	6914	< 1.0	< 0.10
	Tetrahydrofuran	367(1.27)	504	7406	< 1.0	< 0.10
	Ethanol	358(1.29)	503	8052	< 1.0	< 0.10
	Ethyl acetate	354(2.34)	502	8367	< 1.0	< 0.10
	Acetonitrile	359(3.61)	504	8013	< 1.0	< 0.10
L2	Benzene	360(0.45)	520	8547	< 1.0	< 0.10
	Dichloromethane	362(0.80)	522	8467	< 1.0	< 0.10
	Tetrahydrofuran	364(0.83)	521	8278	< 1.0	< 0.10
	Ethanol	360(0.36)	521	8583	< 1.0	< 0.10
	Ethyl acetate	359(1.03)	521	8661	< 1.0	< 0.10
	Acetonitrile	353(1.12)	527	9353	< 1.0	< 0.10

L3	Benzene	356(0.66)	578	10788	6.2	0.99
	Dichloromethane	413(0.64)	576	10263	16.4	2.37
	Tetrahydrofuran	367(0.69)	578	9946	9.0	1.85
	Ethanol	354(0.54)	577	10917	12.6	1.31
	Ethyl acetate	359(1.56)	575	10463	3.8	1.55
	Acetonitrile	353(1.13)	573	10876	6.2	2.01
L4	Benzene	359(0.87)	584	10731	2.2	0.83
	Dichloromethane	362(0.92)	584	10501	5.4	0.85
	Tetrahydrofuran	365(1.23)	582	10215	2.6	0.73
	Ethanol	371(0.88)	585	9860	4.2	0.81
	Ethyl acetate	359(1.47)	583	10702	2.4	0.90
	Acetonitrile	366(1.29)	583	10169	2.8	1.20

a Peak position of the largest absorption band in nm (1.0×10^{-5} mol/L). b Maximum molar absorbance in 10^4 L/mol□cm. c Peak position of SPEF, exited at the absorption maximum. d Stokes shift in cm^{-1}. e Quantum yields was the absolute quantum yields. f The fitted average fluorescence lifetime.

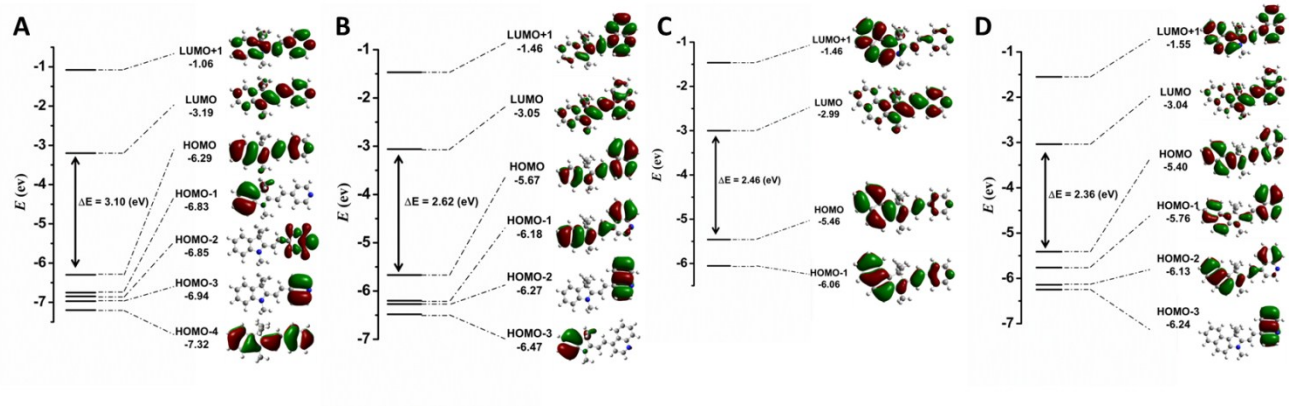

Figure S3. Frontier molecular orbitals of **L1** (A), **L2** (B), and **L4** (C) (optimized geometry).

Table S5. Calculated UV-vis absorption properties, including wavelength (nm), excitation energy (eV), oscillator strengths, and major contribution for **L1**, **L2**, **L3**, and **L4**.

Compounds	Experimental	Calculated data				
	λ_{max}(nm)	λ_{max}(nm)	*E*(eV)	*f* (oscillator strengths)	Composition	Character
L1	367	364	3.402	0.0872	69-71 (H-1→L)	ICT
	296	298	4.148	0.2586	66-71 (H-4→L)	π-$\pi^*_{(indolium)}$
L2	364	365	3.399	0.1045	80-84 (H-3→L)	ICT
	294	290	4.278	0.2193	79-85 (H-4→L+1)	π-$\pi^*_{(indolium)}$
L3	367	398	3.113	0.4882	82-84 (H-1→L)	ICT
	300	295	4.198	0.0988	83-85 (H→L+1)	π-$\pi^*_{(benzoindolium)}$
L4	365	395	3.135	0.2080	94-97 (H-2→L)	ICT
	297	305	4.063	0.0788	96-98 (H→L+1)	π-$\pi^*_{(benzoindolium)}$

Table S6. Calculated emission properties, including wavelength (nm), oscillator strengths, and major contribution for **L1**, **L2**, **L3**, and **L4**.

Compounds	Experimental	Calculated data		
	λ_{max}(nm)	λ_{max}(nm)	*f* (oscillator strengths)	Composition
L1	500	485	1.0070	LUMO→HOMO
L2	510	521	0.4280	LUMO→HOMO
L3	580	603	0.4675	LUMO→HOMO
L4	590	622	0.3814	LUMO→HOMO

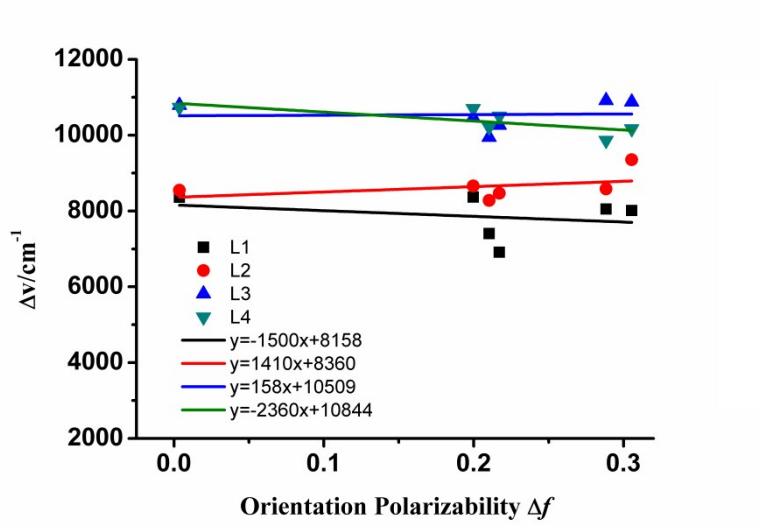

Figure S4. Lippert -Mataga regressions of **L1**, **L2**, **L3**, and **L4** with transition dipole moments 0.46 D, 0.50 D, 0.18 D, and 0.64D, respectively.

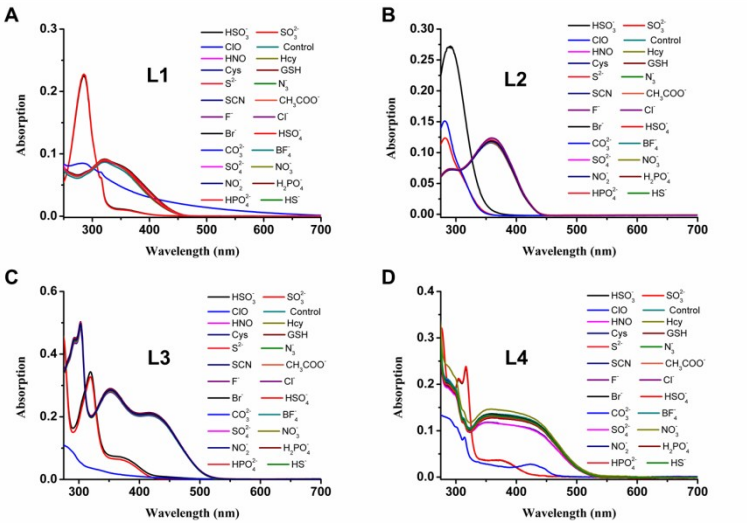

Figure S5. The UV-vis absorption spectra of **L1**-**L4** (1×10^{-5} mol/L) mixed with various anions, and biothiols: HNO, Hcy, Cys, GSH, S_2^-, N_3^-, SCN^-, CH_3COO^-, F^-, Cl^-, Br^-, HSO_4^-, CO_3^{2-}, BF_4^-, SO_4^{2-}, NO_3^-, NO_2^-, $H_2PO_4^-$, HPO_4^{2-}, and HS^- (10 equiv).

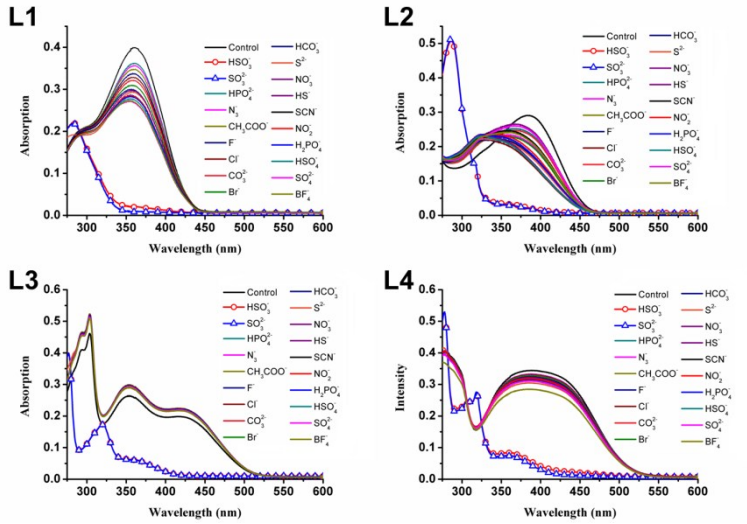

Figure S6. The UV-vis spectra of **L1**, **L2**, **L3**, and **L4** (1×10^{-5} mol/L) mixed with various anions: HSO_3^-, SO_3^{2-}, $H_2PO_4^-$, N_3-, CH_3COO^-, F^-, Cl^-, CO_2^{2-}, Br^-, HCO_3^-, S^{2-}, NO_3^-, HS^-, SCN^-, NO_2^-, $H_2PO_4^-$, HSO4$^-$, SO_4^{2-}, and BF_4^- (1 equv.).

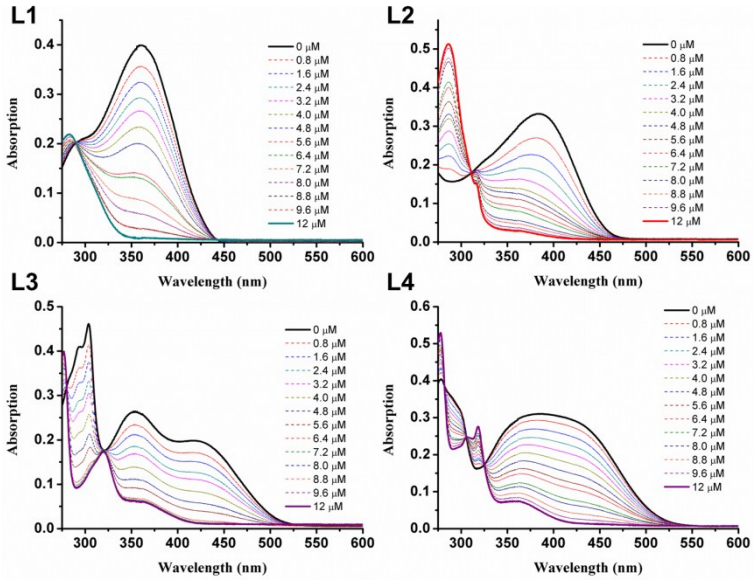

Figure S7. The UV-vis absorption spectra of the four compounds upon titration with increasing concentration of HSO_3^- (0-12 μmol/L) in PBS.

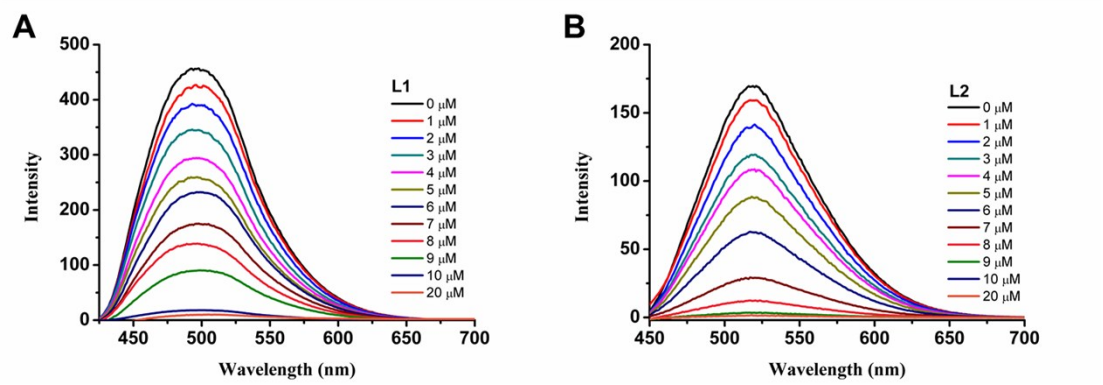

Figure S8. The emission spectra of **L1** and **L2** (c = 10 μM) mixed with different concentrations of HSO_3^- (c = 0 – 20 μM).

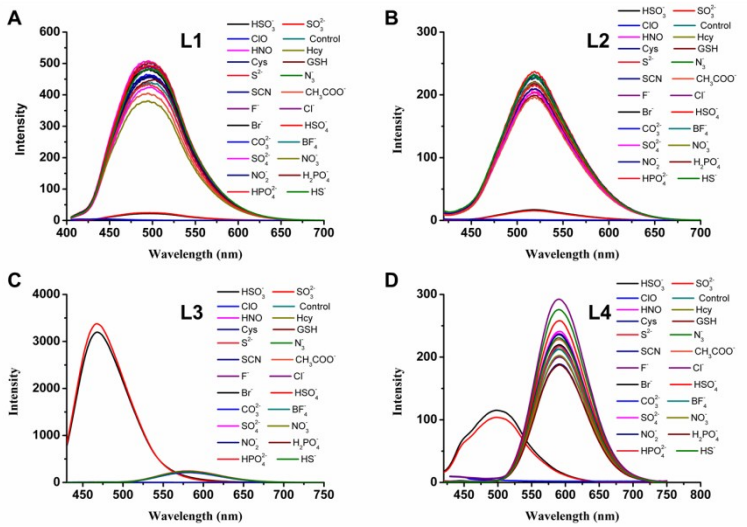

Figure S9. The emission spectra of **L1**-**L4** (10 μM) treated with various anions, and biothiols: HNO, Hcy, Cys, GSH, S_2^-, N_3^-, SCN^-, CH_3COO^-, F^-, Cl^-, Br^-, HSO_4^-, CO_3^{2-}, BF_4^-, SO_4^{2-}, NO_3^-, NO_2^-, $H_2PO_4^-$, HPO_4^{2-}, and HS^- (100 μM, 10 equiv).

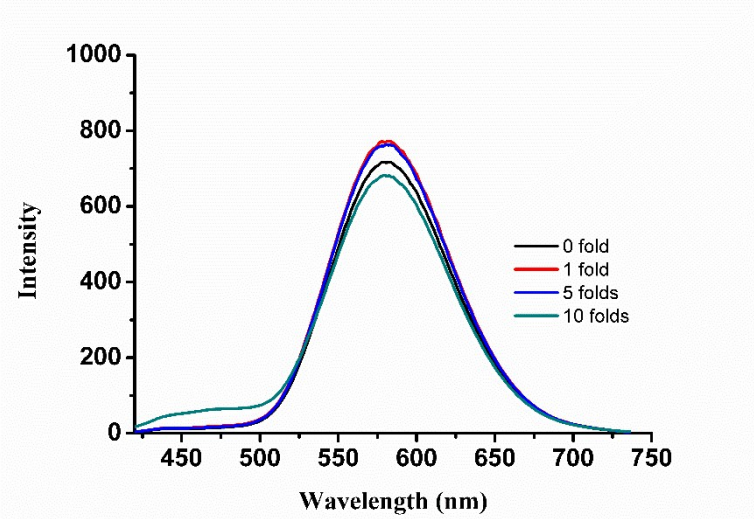

Figure S10. The emission spectra of **L3** (10 μM) treated with different concentration of HS^- (0, 1, 5, 10 folds, after 3 h).

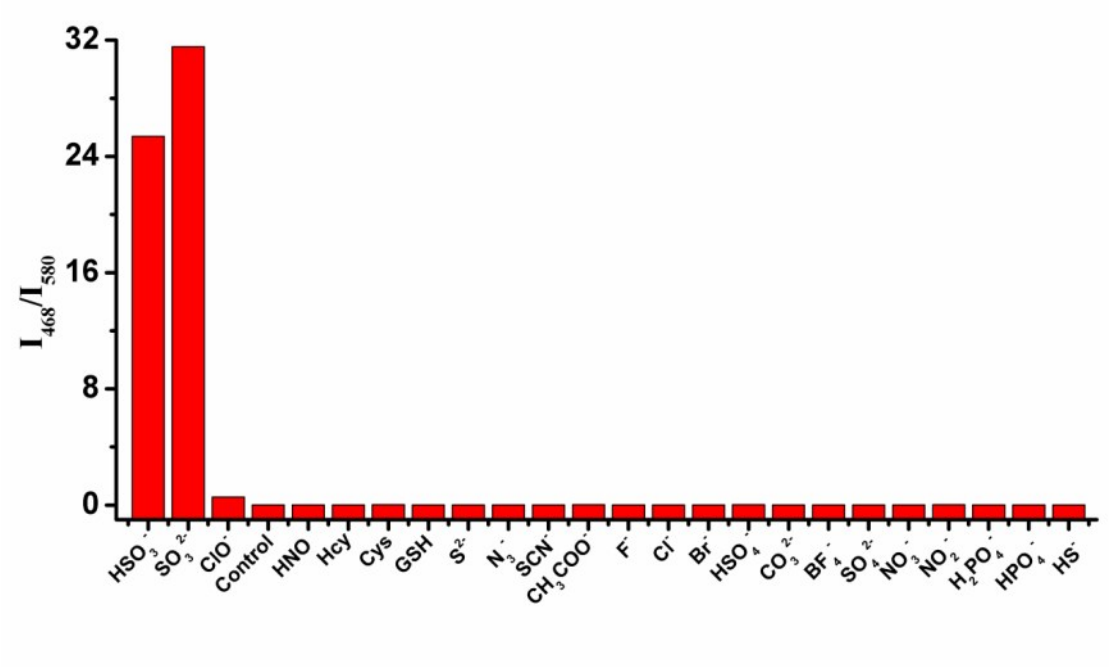

Figure S11. The fluorescence intensity ratios (I_{468}/I_{580}) of **L3** (10 μM) in PBS solutions upon addition of various anions (100μM) and biothoils.

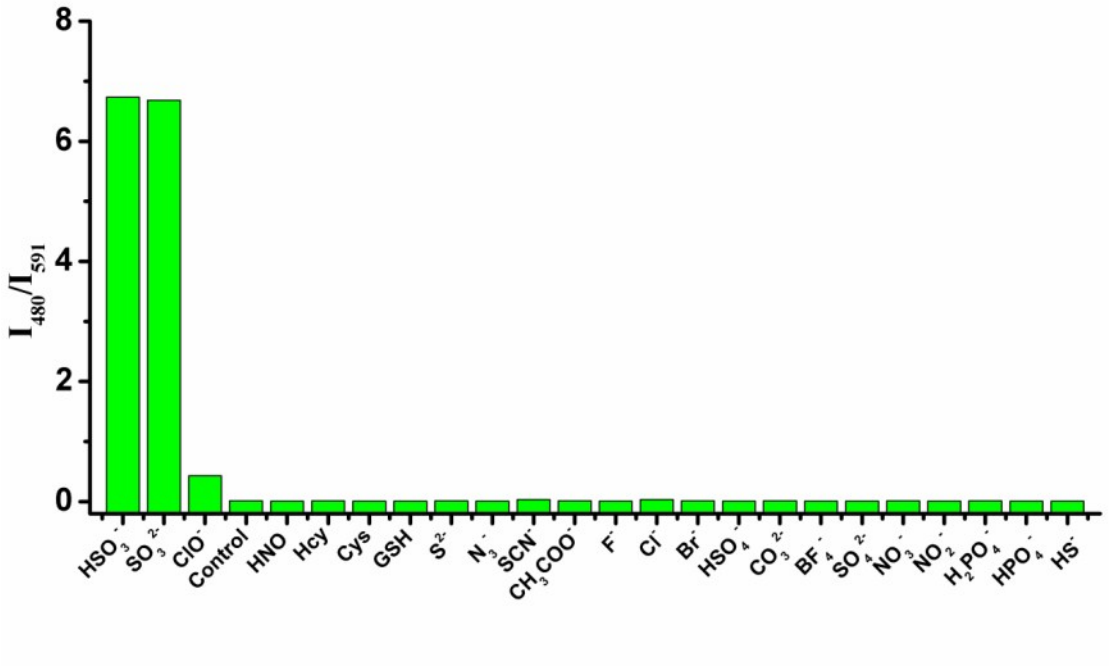

Figure S12. The fluorescence intensity ratios (I_{480}/I_{591}) of **L4** (10 μM) in PBS solutions upon addition of various anions (100μM) and biothoils.

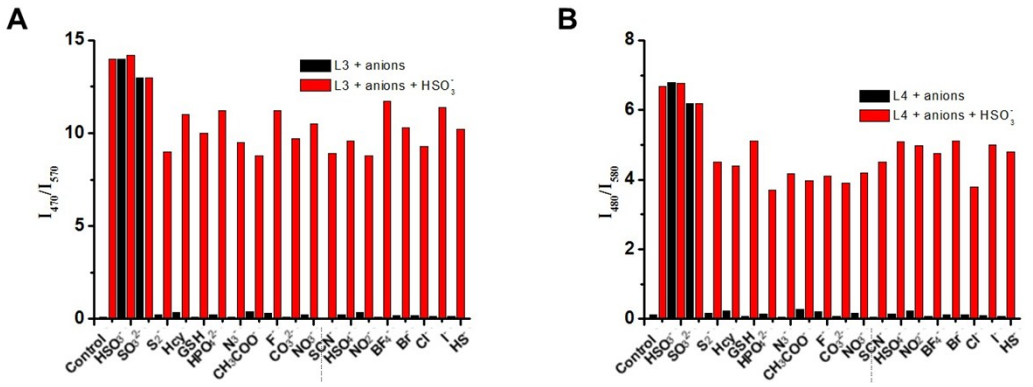

Figure S13. The fluorescence ratio micrograph of **L3** (A) and **L4** (B) in presence of HSO_3^-, SO_3^{2-}, S^{2-}, Hcy, GSH, HPO_4^{2-}, N_3^-, CH_3COO^-, F, CO_3^{2-}, NO_3^-, SCN^-, HSO_4^-, NO_2^-, BF_4^-, Br^-, Cl^-, I^-, and HS^- in PBS solutions. Black bar: **L3** and **L4** +various species. Red bar: **L3** and **L4** +various species + HSO_3^-.

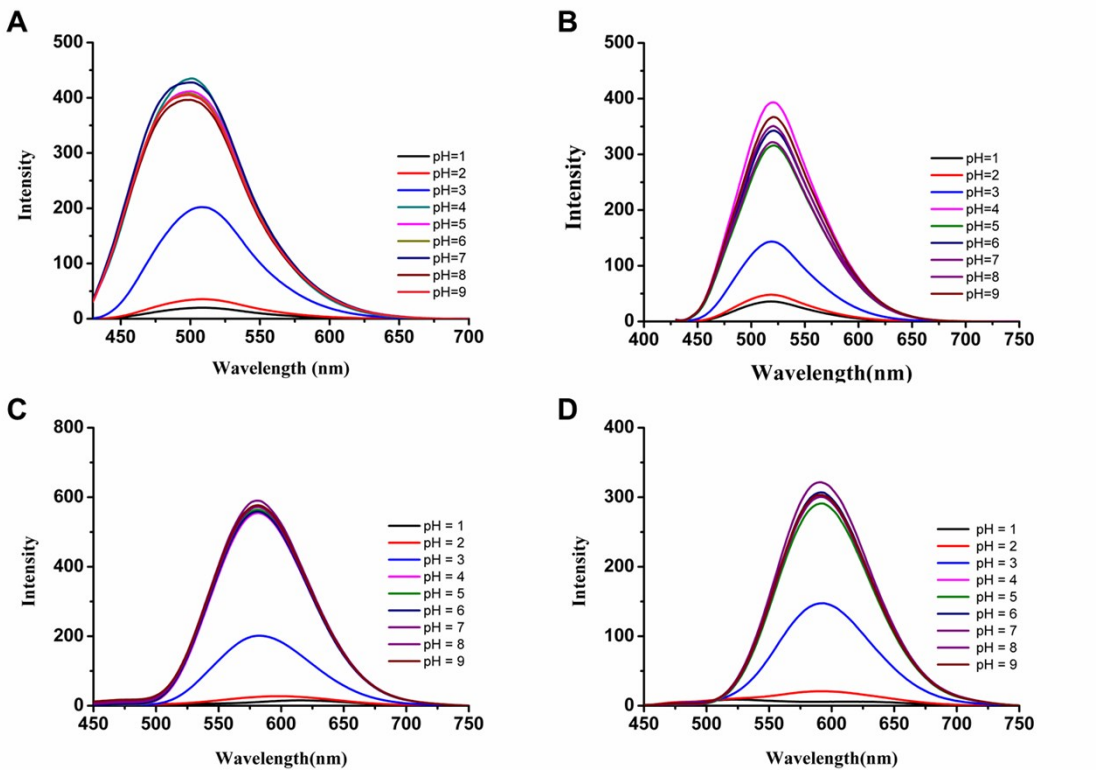

Figure S14. The fluorescent emission spectra of **L1** (A), **L2** (B), **L3** (C) and **L4** (D) in different pH solution (concentration 10 μM).

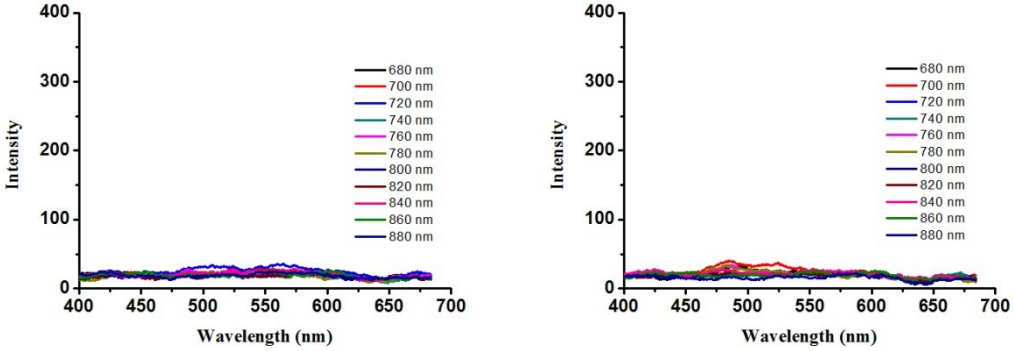

Figure S15. Two-photon excited fluorescence spectra of **L1** (left) and **L2** (right) in acetonitrile with concentration 500 μM from 680-880 nm

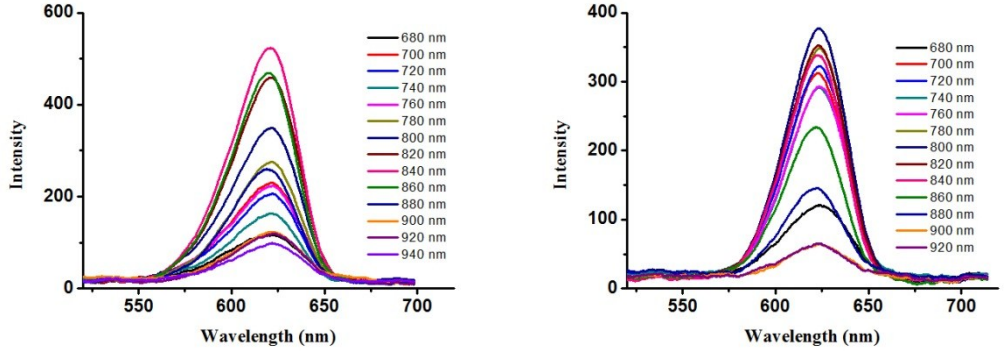

Figure S16. Two-photon excited fluorescence spectra of **L3** (left) and **L4** (right) in acetonitrile with concentration 500 μM from 680 nm to 920 nm

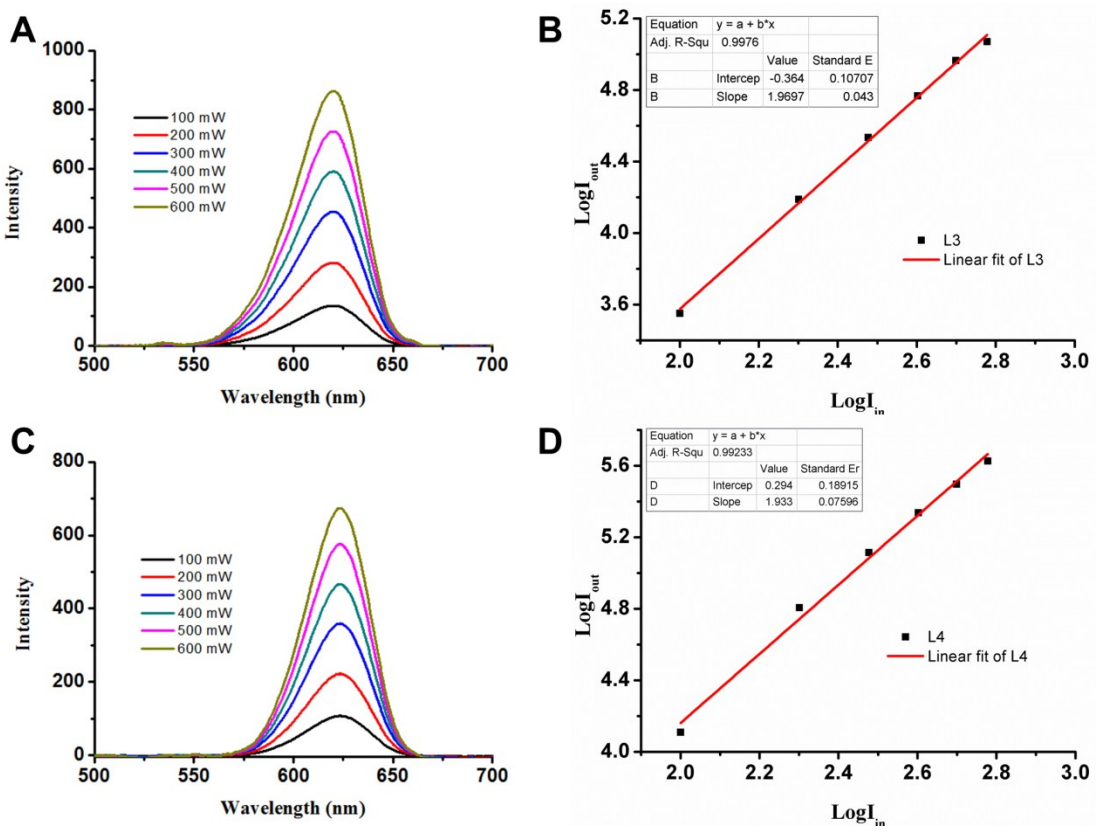

Figure S17. 2PEF spectra of **L3** (A) and **L4** (C) under different pumped powers, with c= 500 μM in acetonitrile; Output fluorescence (I_{out}) vs. the square of input laser power (I_{in}) for **L3** (B) and **L4** (D).

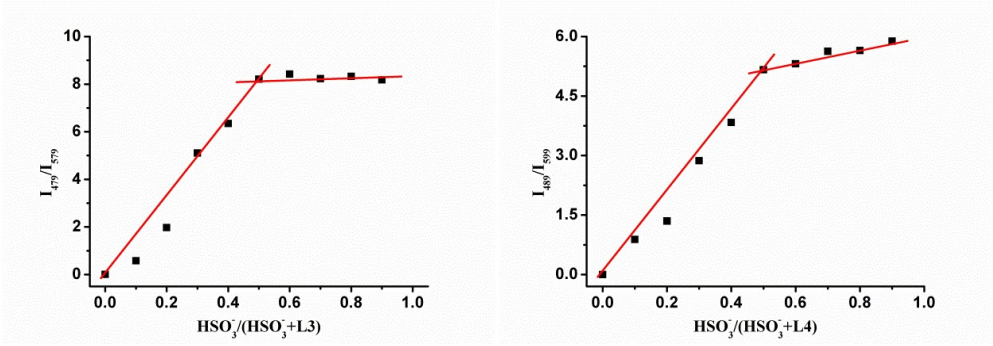

Figure S18. The job plots of **L3** (left)/**L4** (right) and HSO_3^- (λ_{ex} = 365 nm). The total concentration of **L3**/**L4** and HSO_3^- were 10 μM at room-temperature in PBS

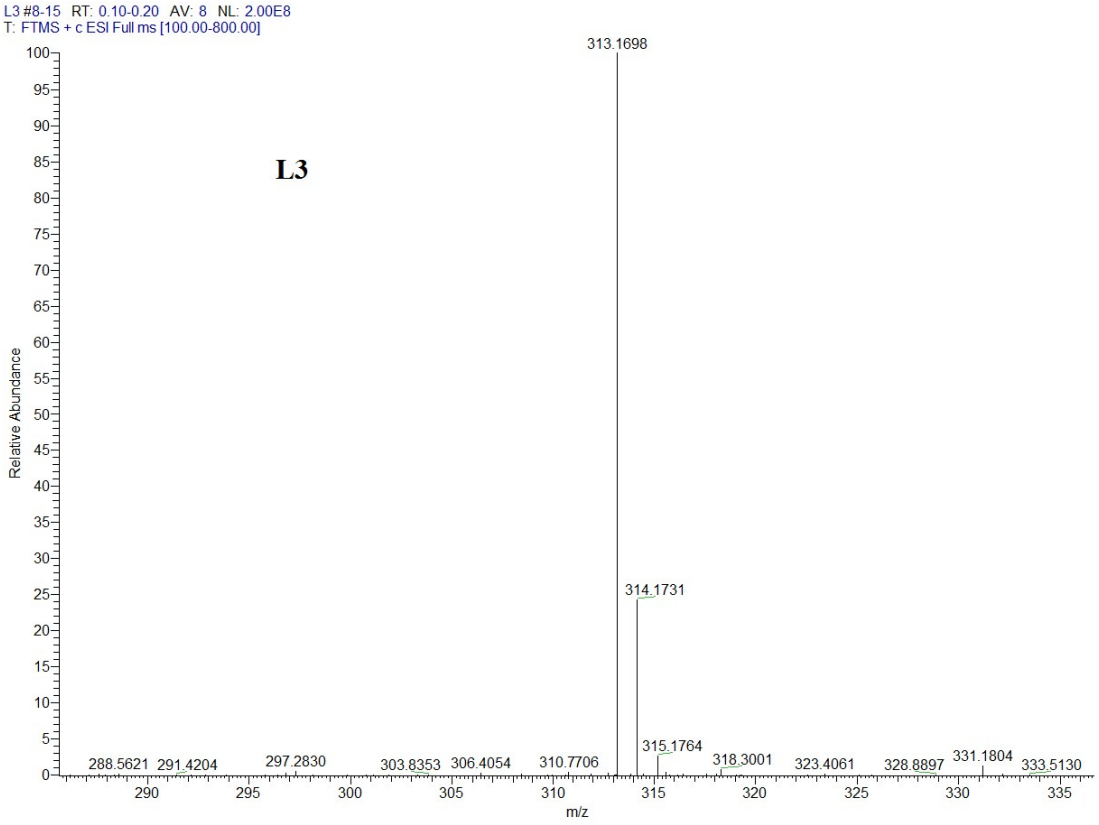
L3 #8-15 RT: 0.10-0.20 AV: 8 NL: 2.00E8
T: FTMS + c ESI Full ms [100.00-800.00]
L3
313.1698
314.1731
315.1764
288.5621
291.4204
297.2830
303.8353
306.4054
310.7706
318.3001
323.4061
328.8897
331.1804
333.5130
Relative Abundance
m/z

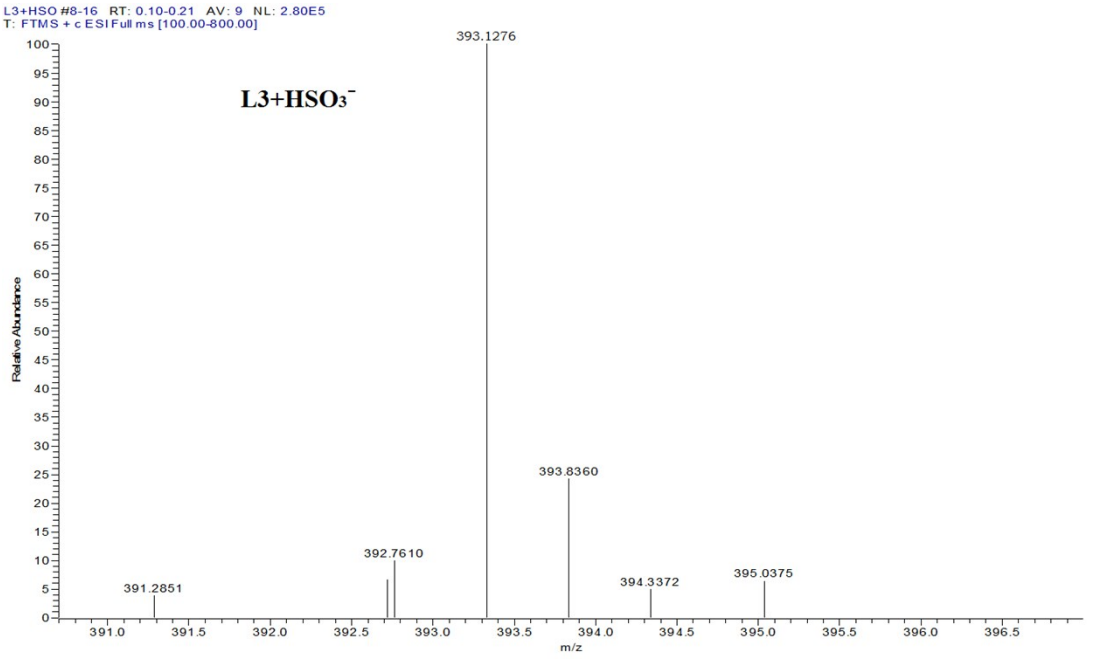
L3+HSO #8-16 RT: 0.10-0.21 AV: 9 NL: 2.80E5
T: FTMS + c ESI Full ms [100.00-800.00]
L3+HSO3-
393.1276
393.8360
392.7610
391.2851
394.3372
395.0375
Relative Abundance
m/z

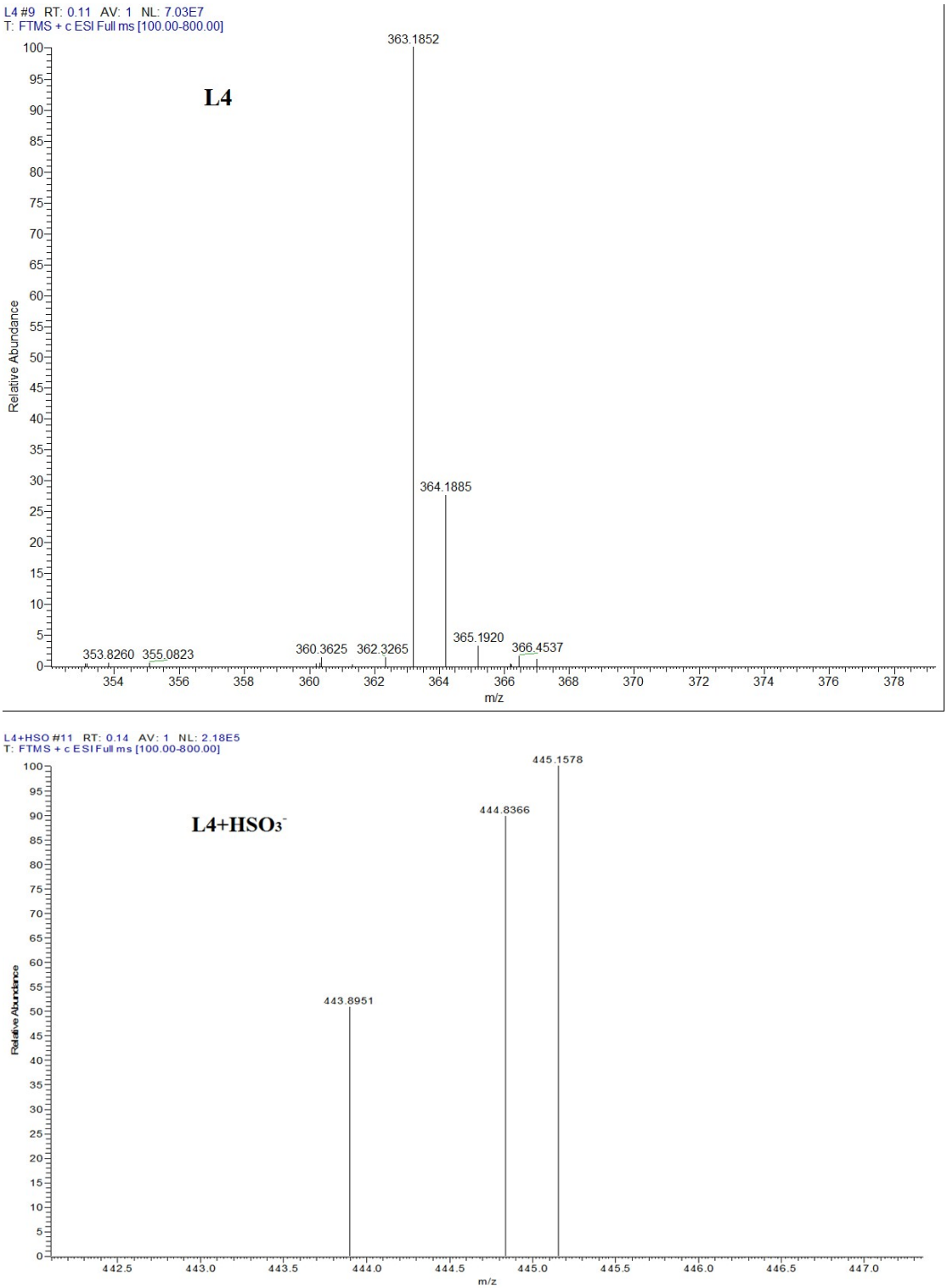

Figure S19. The original ESI-MS spectra of **L3**, **L3**+HSO_3^-, **L4**, and **L4**+HSO_3^-.

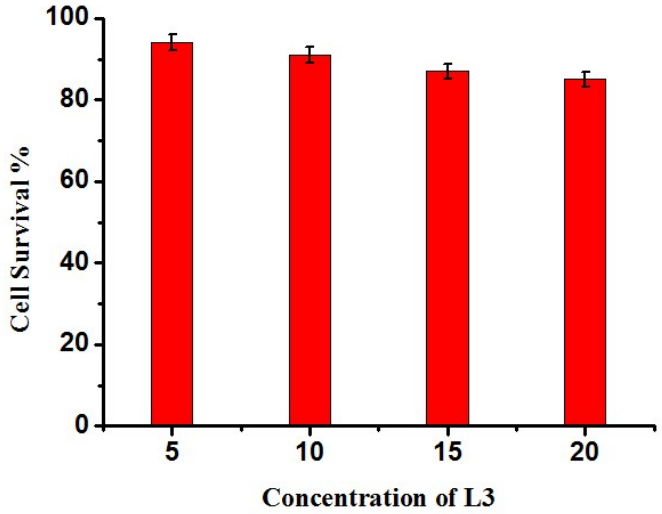

Figure S20. The cell survival of HepG2 cells incubated with different concentration of **L3** by MTT analysis (5-20 μM)

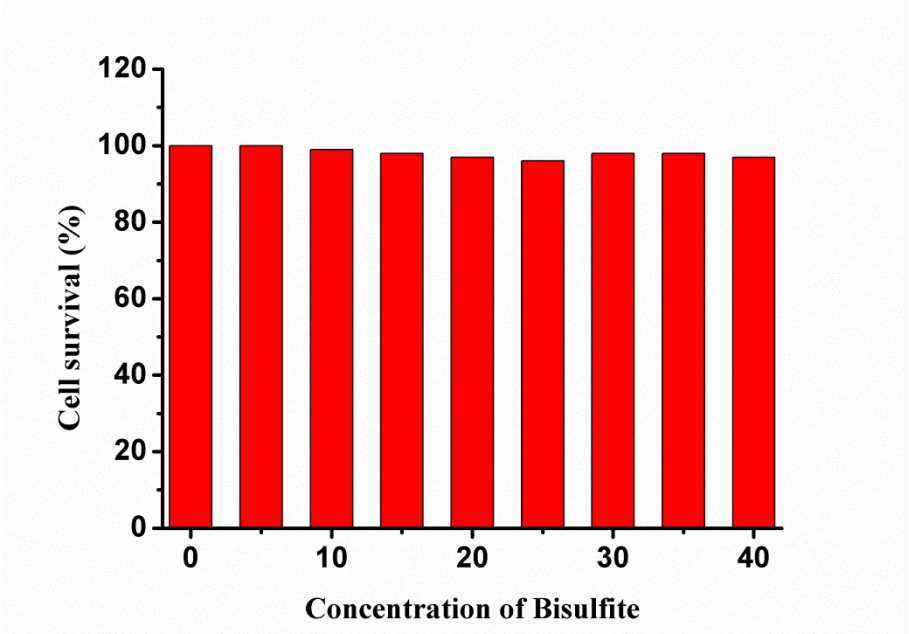

Figure S21. The cell survival of HepG2 cells incubated with different concentration of $NaHSO_3$ by MTT analysis (0-40 μM)

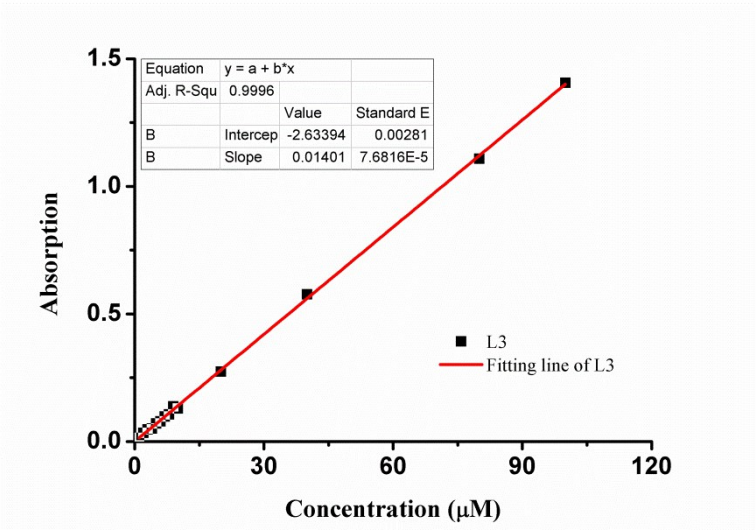

Figure S22. The solubility of **L3** in PBS with various concentrations (1 – 100 μM)

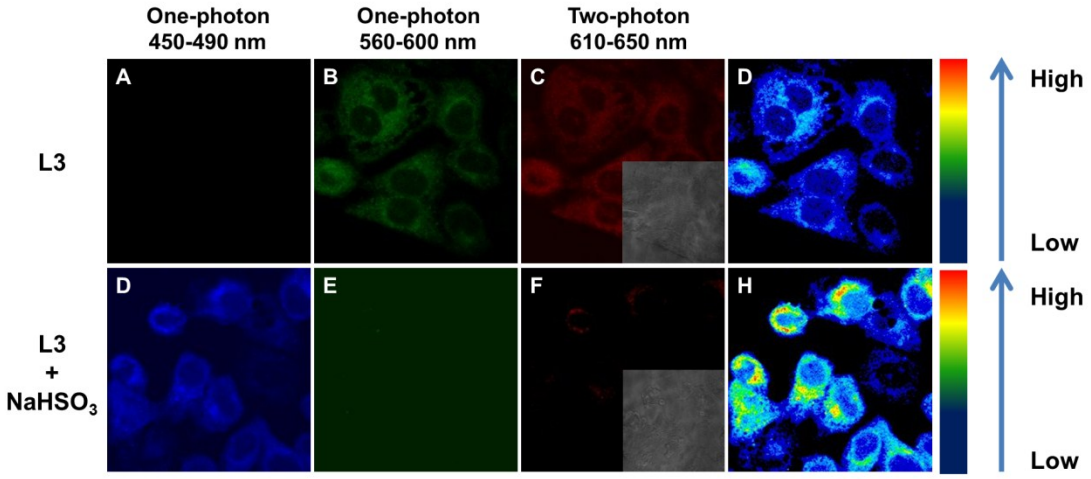

Figure S23. Confocal fluorescence imaging of Hela cells incubated with **L3** for 10 min (A-E), HepG2 cells pre-treated with **L3** for 10 min and incubated with $NaHSO_3$ (20 μM) for 10 min (F-J). A and D were the one-photon excited optical window with emission signal at 450-490 nm; B and E were the one-photon excited optical window with emission signal at 560-600 nm; C and F were two-photon excited optical window with emission signal at 610-650 nm; D and I were the bright field; D and H were the ratio image of **L3** obtained by Image J software.

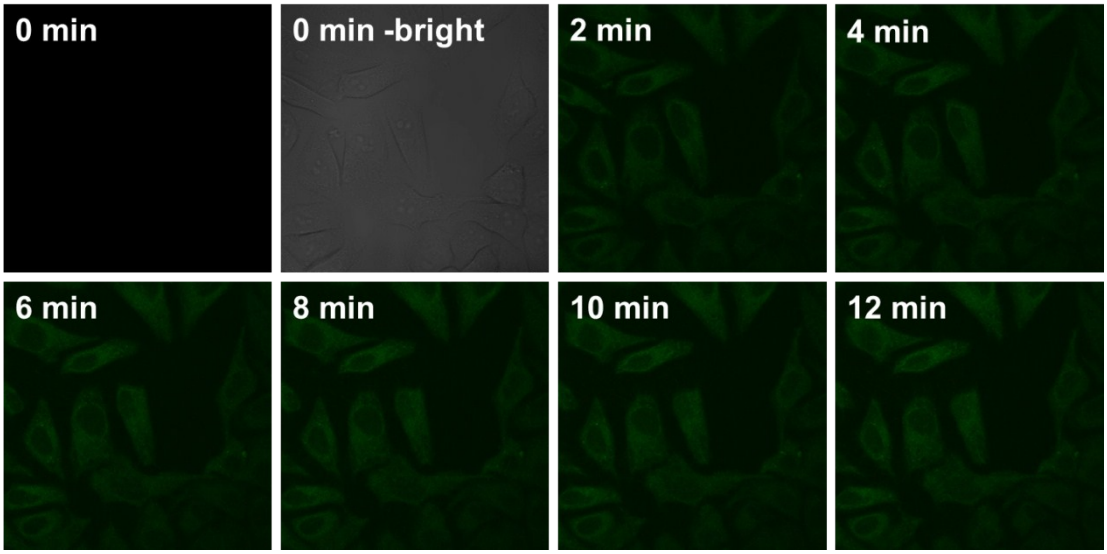

Figure S24. The confocal fluorescence imaging of HepG2 cells incubated with **L3** at different times (0 min, 2 min, 4 min, 6 min, 8 min, 10 min, 12 min)

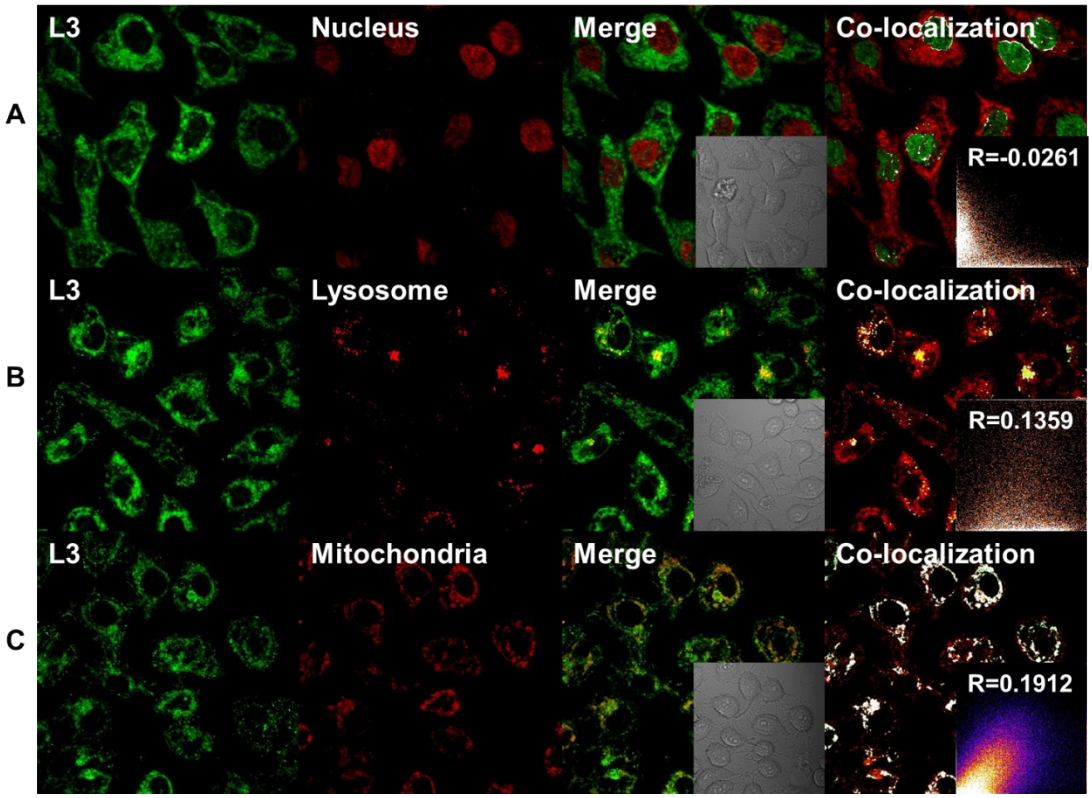

Figure S25. The co-localization imaging microscopies of **L3** with commercial dyes, NucRed™ Live 647 (A), Lysotracker®Red (B), Mitotracker®Red (C).

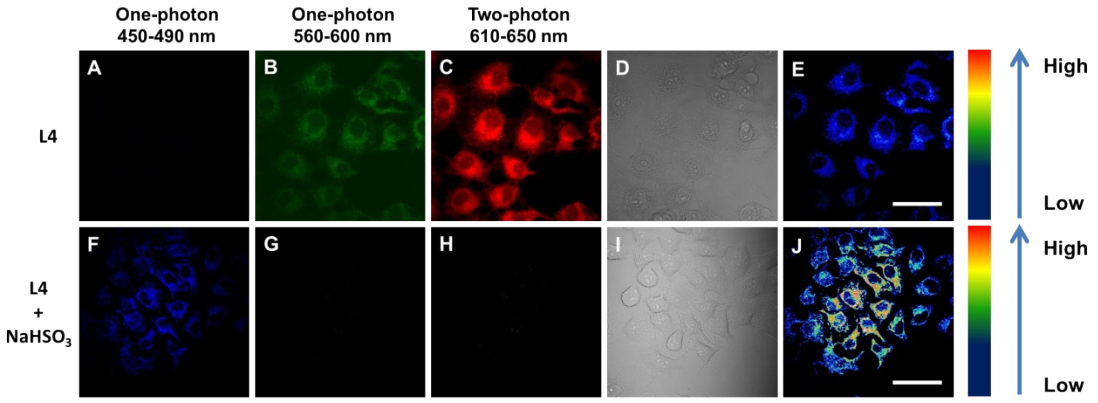

Figure S26. Confocal fluorescence imaging of HepG2 cells incubated with **L4** for 10 min (A-E), HepG2 cells pre-treated with **L4** for 10 min and incubated with $NaHSO_3$ (20 μM) for 10 min (F-J). A and F were the one-photon excited optical window (λ_{ex} = 405 nm) with emission signal at 450-490 nm; B and G were the one-photon excited optical window with emission signal at 560-600 nm; C and H were two-photon excited optical window (λ_{ex} = 840 nm) with emission signal at 610-650 nm; D and I were the bright field; E and J were the ratio image of **L4** obtained by Image J software.

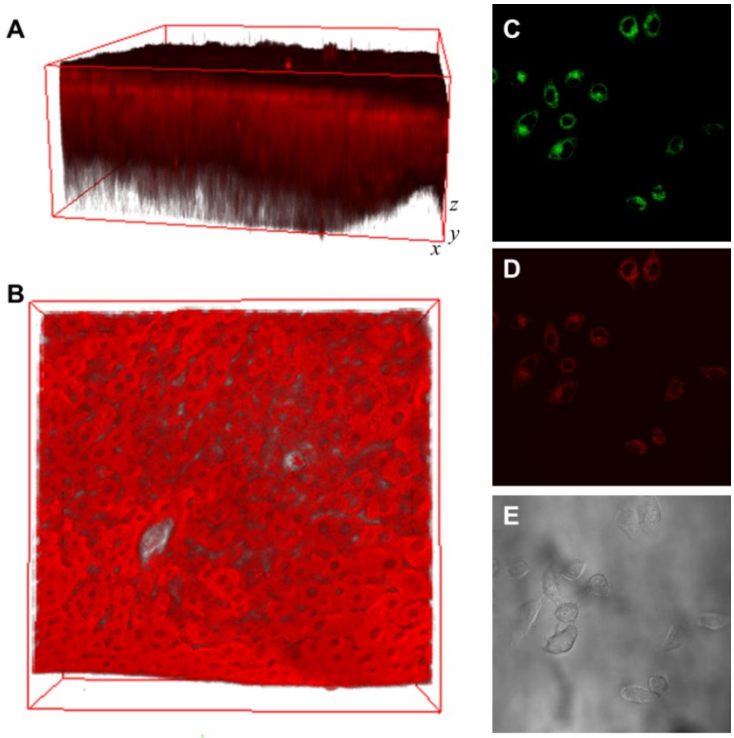

Figure S27. The two-photon excited microscopy imaging for liver (A, with depth *z* = 200 μm, cultured with **L3** for 30 min). The x-y plane of liver (B). One-photon (C), two-photon (D), and bright field (E) imaging of cells with 10 μM **L3** for 10 min.

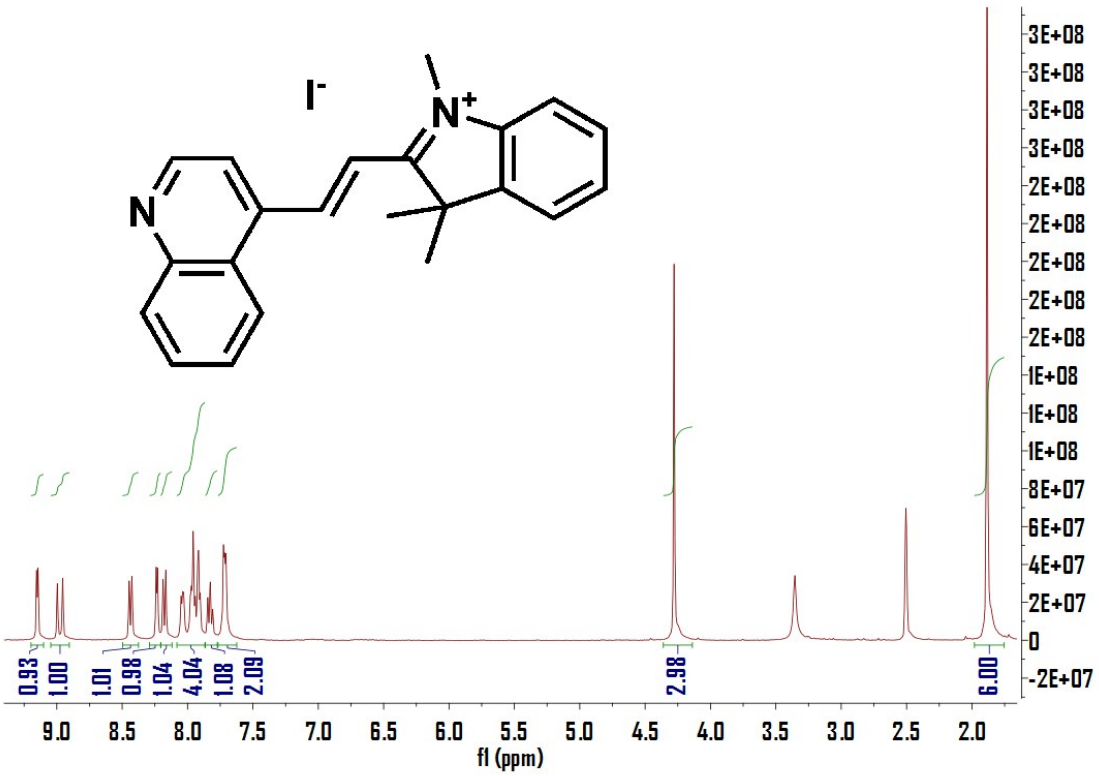
I-
N+
N
0.93
1.00
1.01
0.98
1.04
4.04
1.08
2.09
2.98
6.00
f1 (ppm)

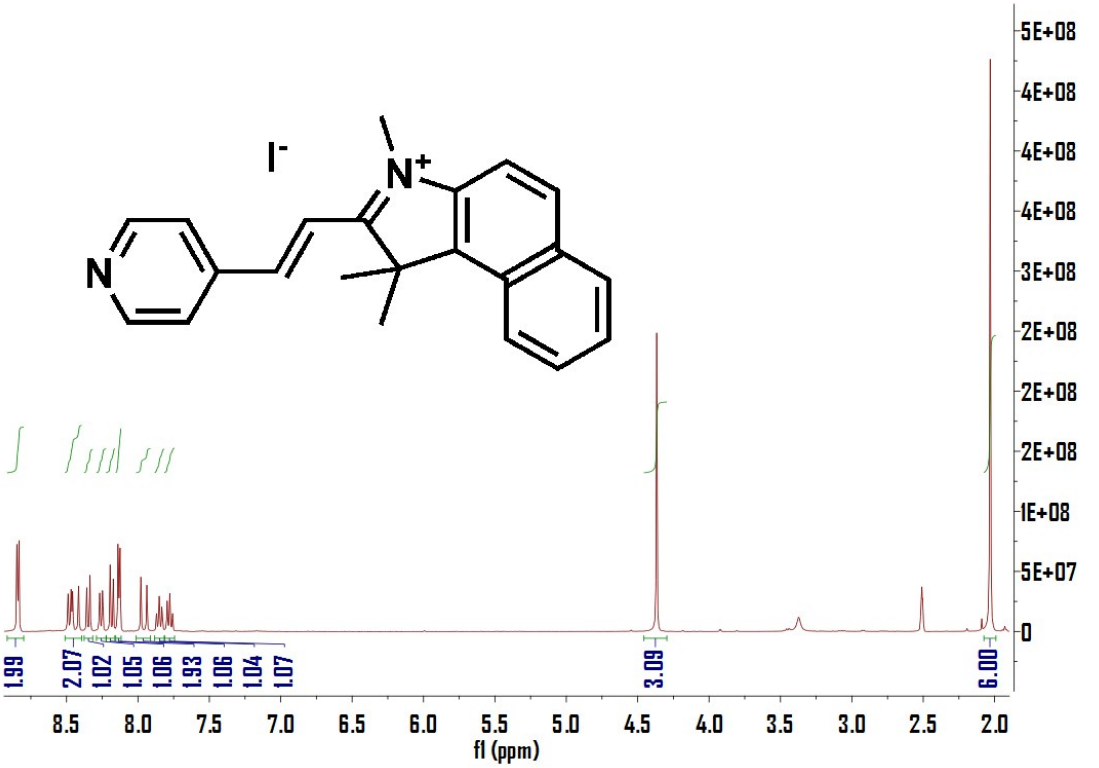
I-
N+
N
1.99
2.07
1.02
1.05
1.06
1.93
1.06
1.04
1.07
3.09
6.00
f1 (ppm)

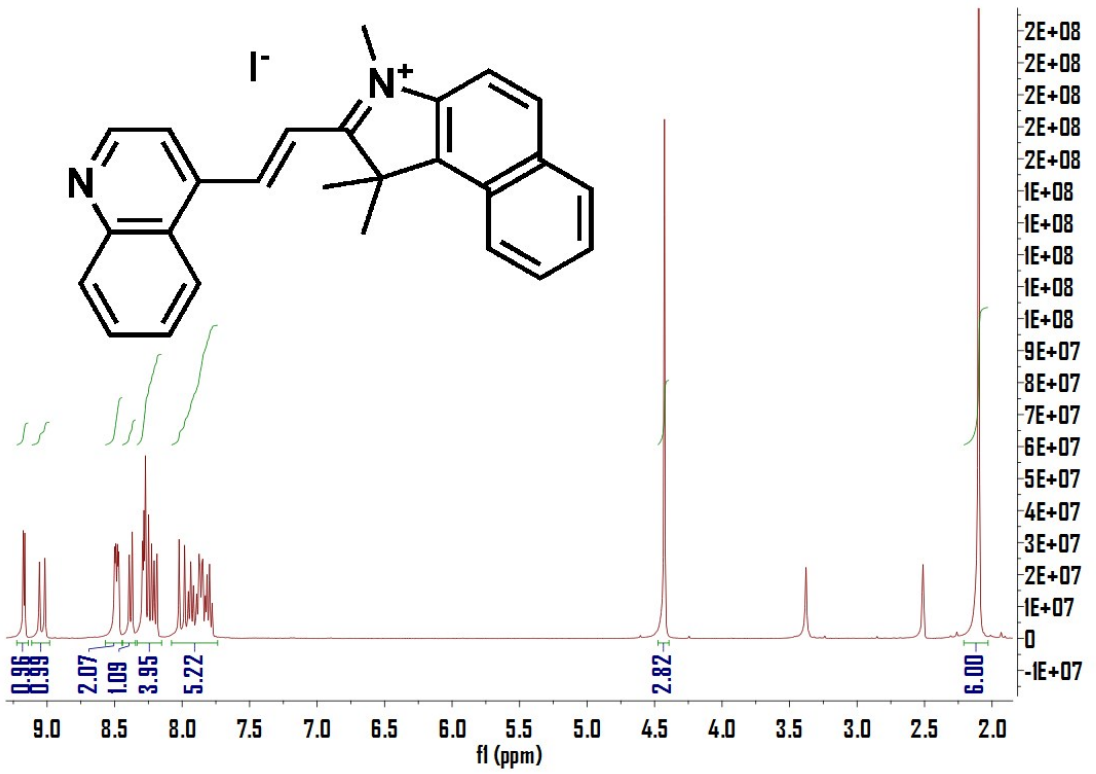

Figure S28. The ^{1}H NMR spectra of L1-L4 in d_6-DMSO

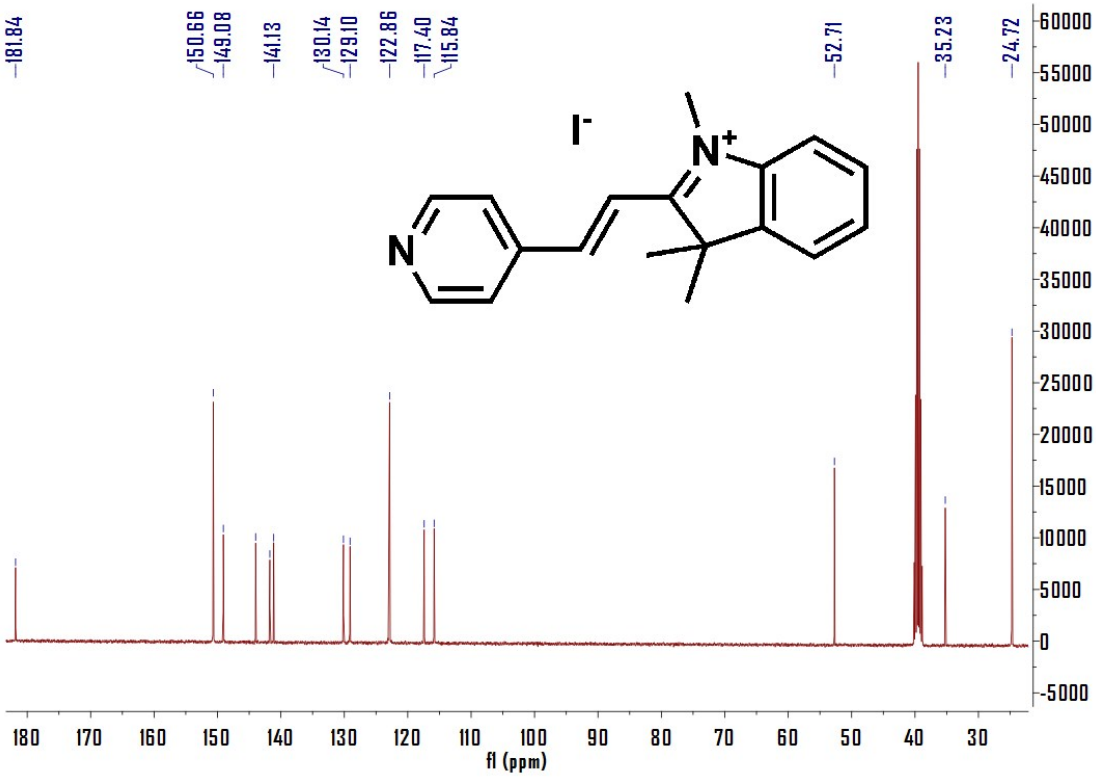

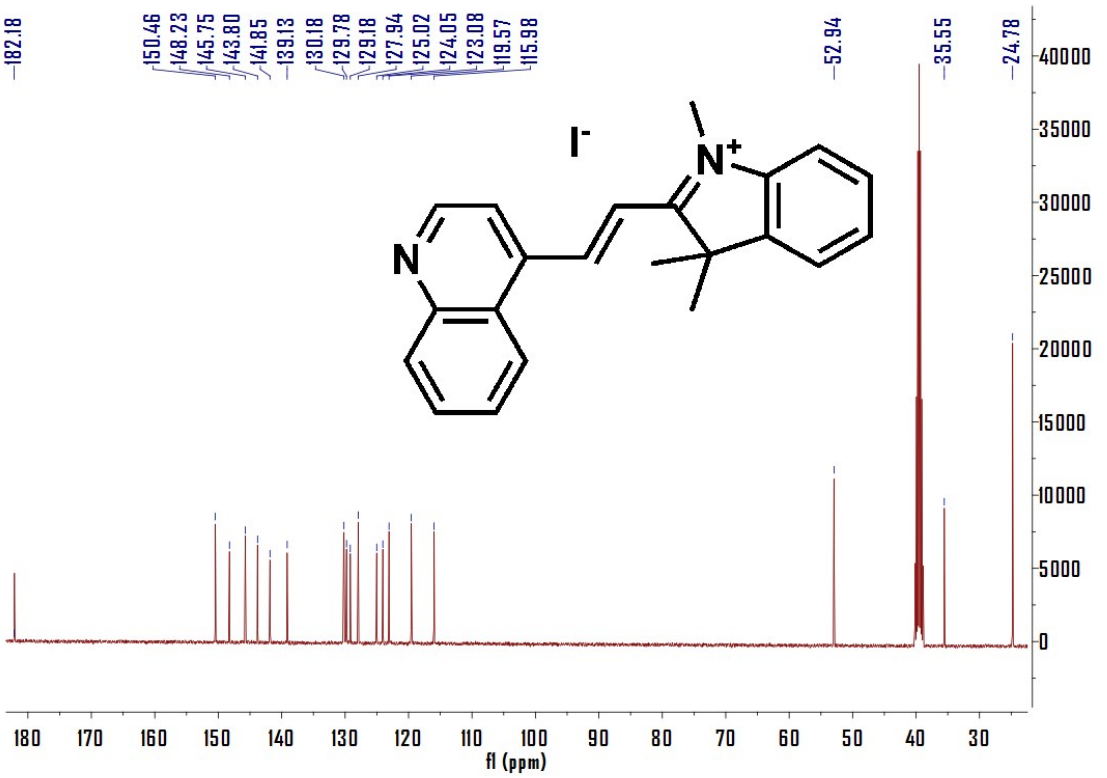
182.18
150.46
148.23
145.75
143.80
141.85
139.13
130.18
129.78
129.18
127.94
125.02
124.05
123.08
119.57
115.98
52.94
35.55
24.78
I-
N+
N
40000
35000
30000
25000
20000
15000
10000
5000
0
180 170 160 150 140 130 120 110 100 90 80 70 60 50 40 30
f1 (ppm)

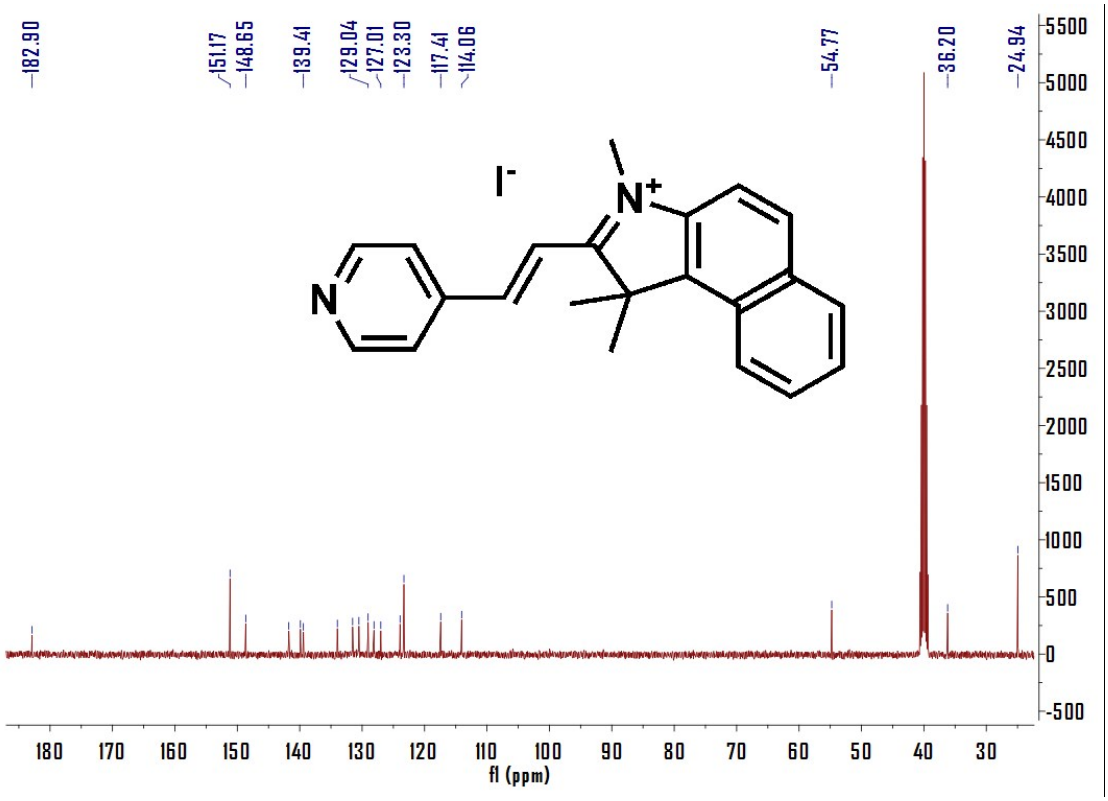
182.90
151.17
148.65
139.41
129.04
127.01
123.30
117.41
114.06
54.77
36.20
24.94
I-
N+
N
5500
5000
4500
4000
3500
3000
2500
2000
1500
1000
500
0
-500
180 170 160 150 140 130 120 110 100 90 80 70 60 50 40 30
f1 (ppm)

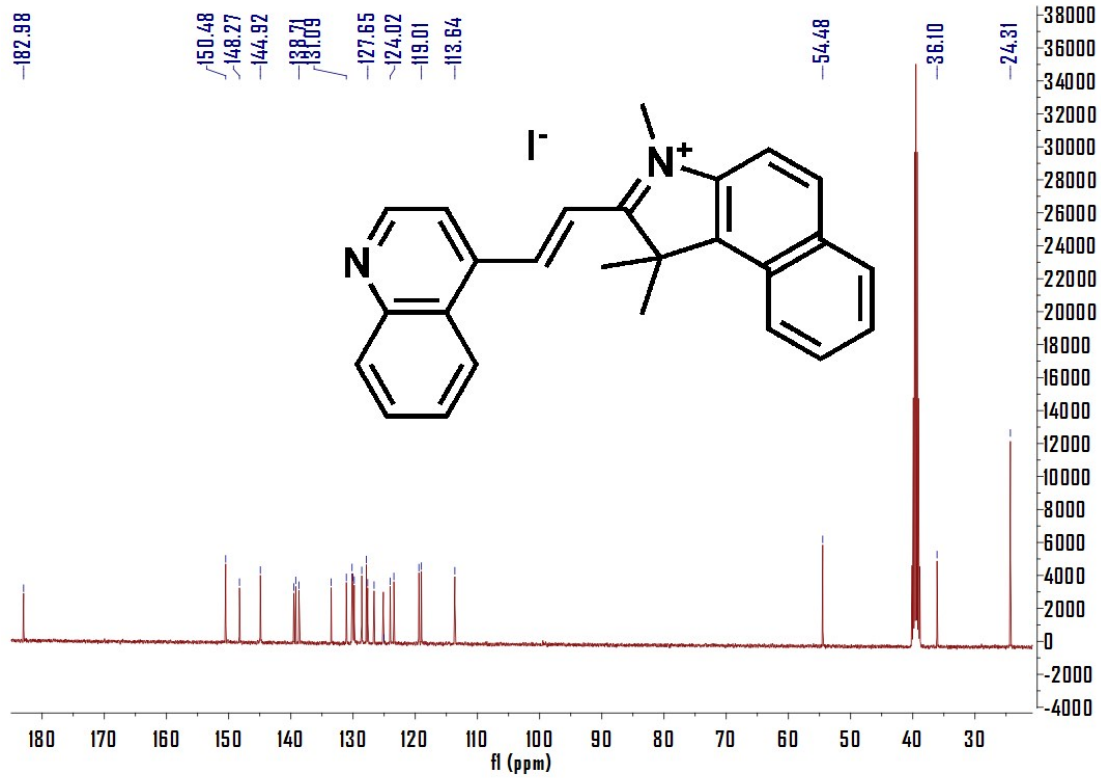

Figure S29. The ^{13}C NMR spectra of L1-L4 in d_6-DMSO

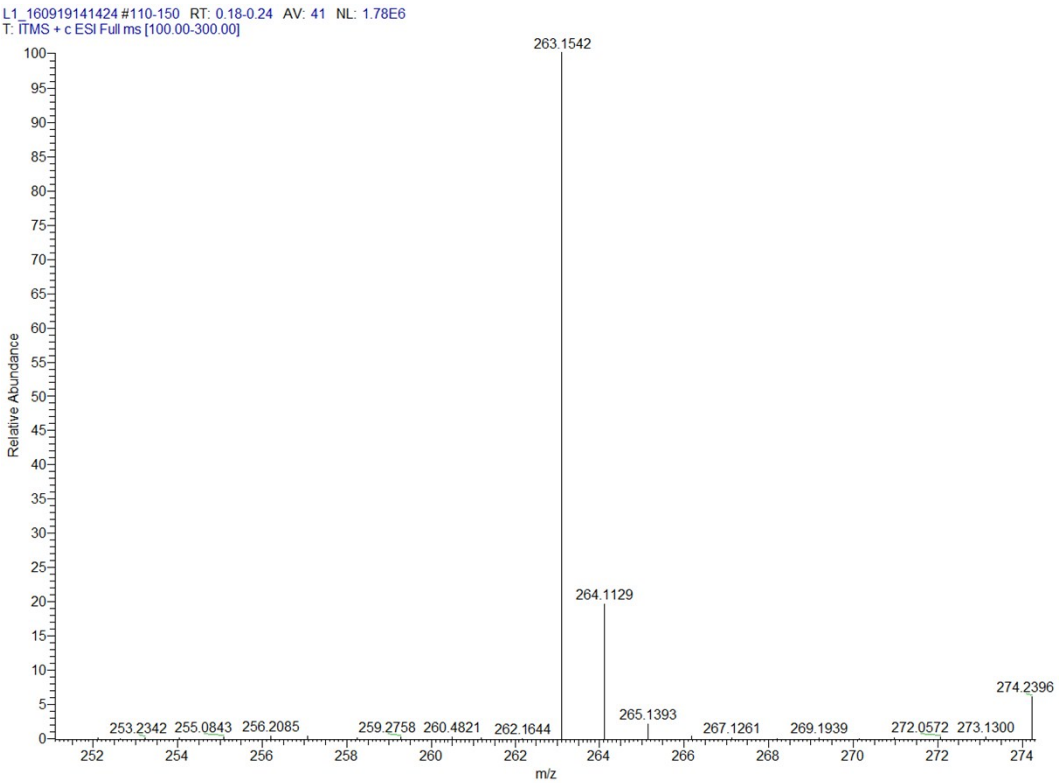

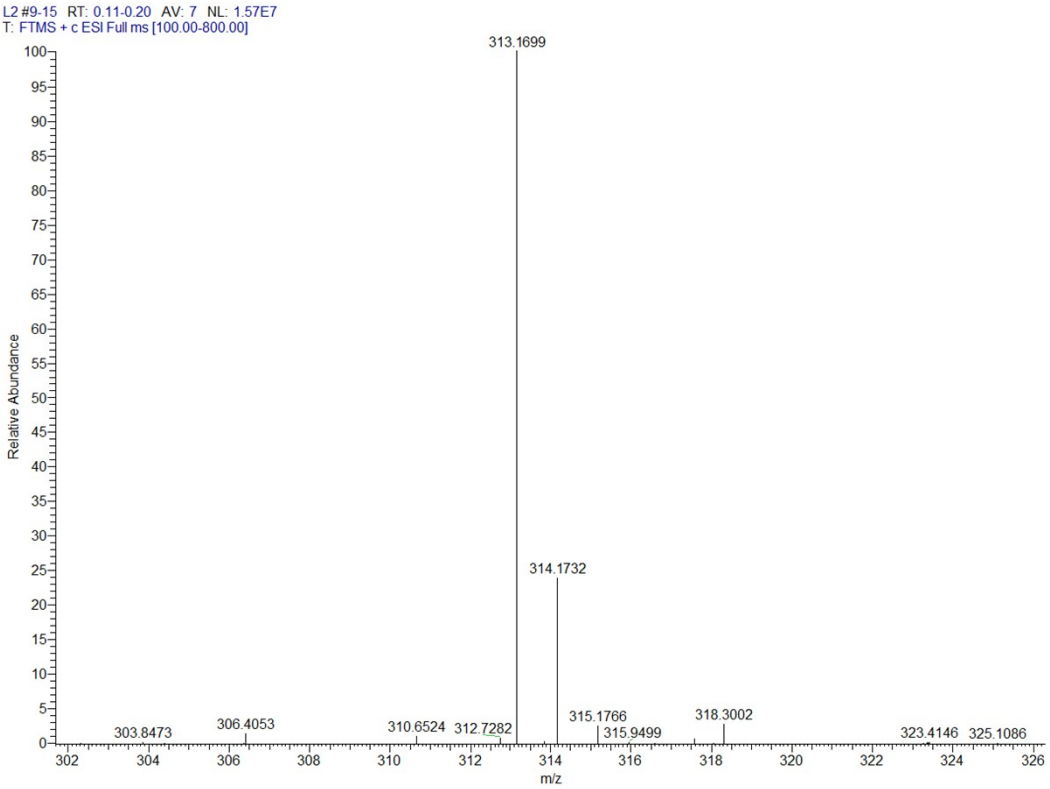
L2 #9-15 RT: 0.11-0.20 AV: 7 NL: 1.57E7
T: FTMS + c ESI Full ms [100.00-800.00]
313.1699
314.1732
315.1766
318.3002
315.9499
303.8473
306.4053
310.6524
312.7282
323.4146
325.1086
Relative Abundance
m/z

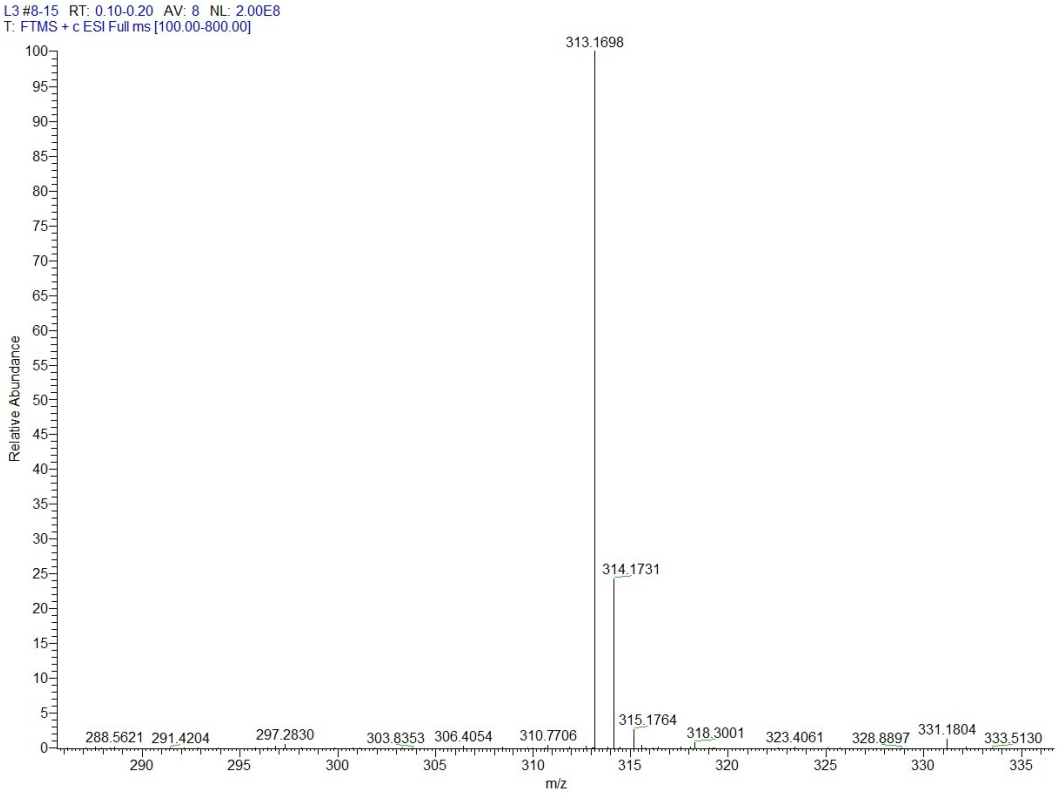
L3 #8-15 RT: 0.10-0.20 AV: 8 NL: 2.00E8
T: FTMS + c ESI Full ms [100.00-800.00]
313.1698
314.1731
315.1764
318.3001
288.5621
291.4204
297.2830
303.8353
306.4054
310.7706
323.4061
328.8897
331.1804
333.5130
Relative Abundance
m/z

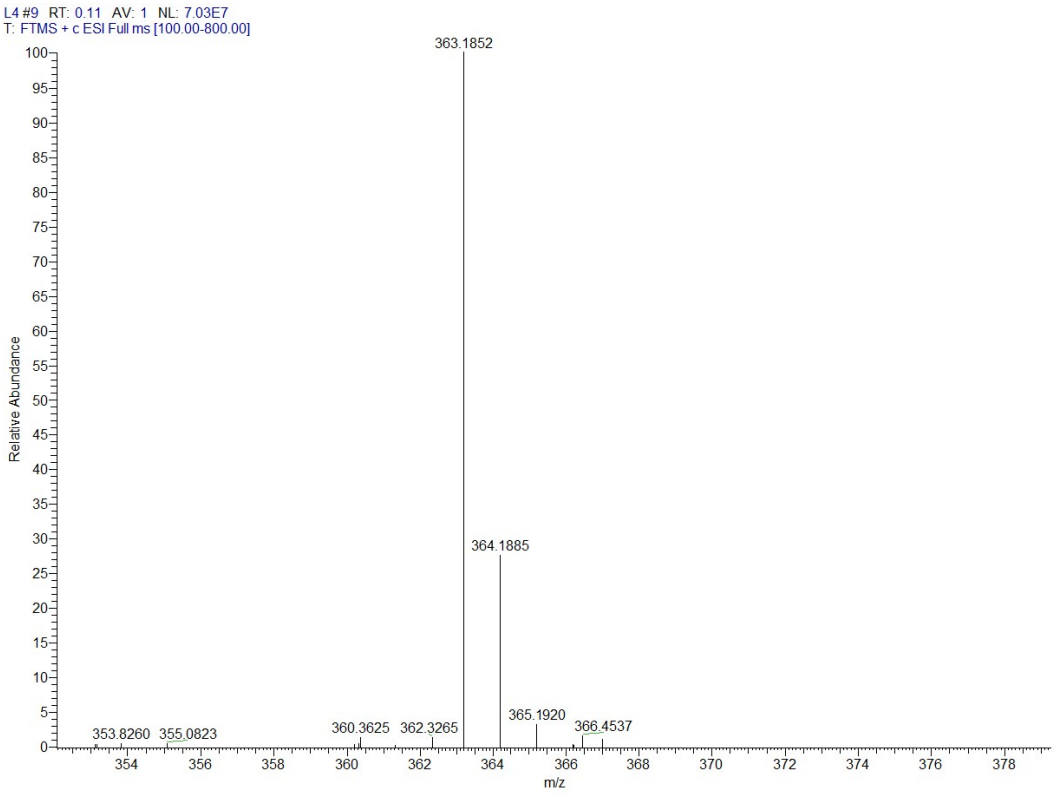

Figure S30. The ESI-MS spectra of **L1-L4**.